Journal Pre-proof

Emission colour changes in the CaF_2 sub-microspheres doped with Yb^{3+}, Er^{3+} and Mn^{2+} ions

Agata Szczeszak, Tomasz Grzyb, Grzegorz Nowaczyk, Anna Ekner-Grzyb

PII: S0925-8388(19)33964-7

DOI: https://doi.org/10.1016/j.jallcom.2019.152718

Reference: JALCOM 152718

To appear in: *Journal of Alloys and Compounds*

Received Date: 21 June 2019

Revised Date: 16 October 2019

Accepted Date: 17 October 2019

Please cite this article as: A. Szczeszak, T. Grzyb, G. Nowaczyk, A. Ekner-Grzyb, Emission colour changes in the CaF_2 sub-microspheres doped with Yb^{3+}, Er^{3+} and Mn^{2+} ions, *Journal of Alloys and Compounds* (2019), doi: https://doi.org/10.1016/j.jallcom.2019.152718.

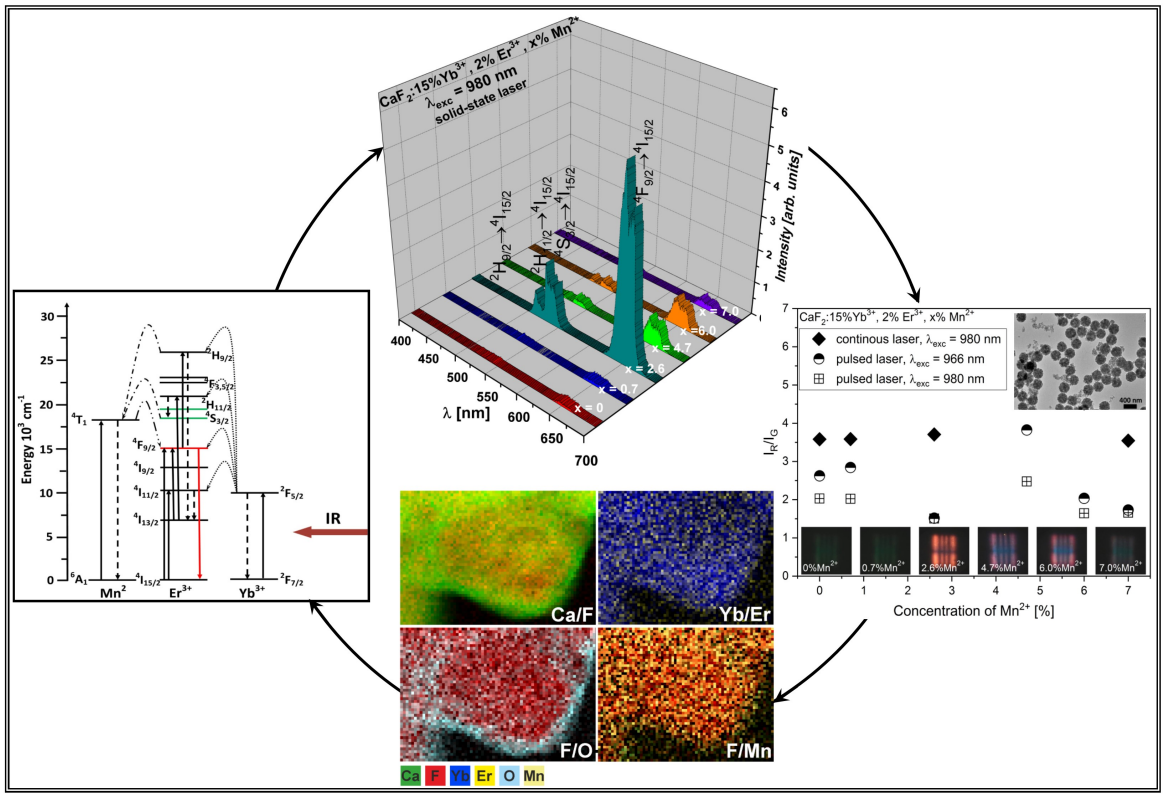
CaF2:15%Yb3+, 2% Er3+, x% Mn2+
λexc = 980 nm
solid-state laser
Intensity [arb. units]
λ [nm]
x = 7.0
x = 6.0
x = 4.7
x = 2.6
x = 0.7
x = 0
Energy 10^3 cm^-1
IR
Mn2
Er3+
Yb3+
CaF2:15%Yb3+, 2% Er3+, x% Mn2+
continous laser, λexc = 980 nm
pulsed laser, λexc = 966 nm
pulsed laser, λexc = 980 nm
IF/IG
Concentration of Mn2+ [%]
0%Mn2+
0.7%Mn2+
2.6%Mn2+
4.7%Mn2+
6.0%Mn2+
7.0%Mn2+
Ca/F
Yb/Er
F/O
F/Mn
Ca F Yb Er O Mn

Emission colour changes in the CaF_2 sub-microspheres doped with Yb^{3+}, Er^{3+} and Mn^{2+} ions

Agata Szczeszak[a]*, Tomasz Grzyb[a], Grzegorz Nowaczyk[b] and Anna Ekner-Grzyb[c]*

[1]*Adam Mickiewicz University, Faculty of Chemistry, Department of Rare Earths, Uniwersytetu Poznańskiego 8, 61-614 Poznań, Poland*

[2]*Nanobiomedical Centre at Adam Mickiewicz University, Wszechnicy Piastowskiej 3, 61-614 Poznań, Poland*

[3] *Adam Mickiewicz University, Faculty of Biology, Department of Plant Ecophysiology, Faculty of Biology, Uniwersytetu Poznańskiego 6, 61-614 Poznań, Poland*

Abstract

A series of CaF_2-doped phosphors was synthesized *in situ* in hydrothermal conditions (in a DAB- 2 reactor), in the presence of sodium citrate as a complexing agent preventing premature precipitation. The materials were doped with Yb^{3+}/Er^{3+} pair of ions, which resulted in up-conversion emission. Additionally, Mn^{2+} ions were incorporated into the structure of the CaF_2 to analyse their influence on the chromaticity of the luminescence colour, in view of their application in bioimaging. Detailed structural analysis showed that the structure of the nanoparticles obtained resembled the core@shell like structure. Finally, the emission colour was tuned from green to orange – red. It was confirmed that the quantity of Mn^{2+} ions incorporated in the CaF_2 matrix definitely differs from the expected one. The real concentration of Mn^{2+} ions in the structure is frequently ignored, which leads to incorrect conclusions. For this reason, a detailed structural and spectroscopic analysis was conducted and the effect of Mn^{2+} ions on the structure and the average size of the CaF_2-doped phosphors was studied. Moreover, the *in vitro* cytotoxicity of the nanoparticles was evaluated. Obtained results showed that CaF_2:15%Yb^{3+}, 2%Er^{3+}, 2.6%Mn^{2+} reduces cell viability of fibroblast at lower concentrations (50, 100 and 200 µg/ml) than CaF_2:15%Yb^{3+}, 2%Er^{3+} (200 µg/ml). Moreover, CaF_2:15%Yb^{3+}, 2%Er^{3+} caused increase of the fibroblast proliferation rate at the lowest tested concentration (10 µg/ml).

Keywords: upconversion, luminescence, lanthanides, calcium fluoride, Mn^{2+} ions, hydrothermal method

Introduction

These days much attention is paid to phosphors exhibiting up-conversion phenomenon which is of interest in many fields including fluorescence labelling [1], multilevel anti-counterfeiting [2], temperature sensors [3–5], theranostic systems [6] or photodynamic cancer therapy [7]. From the spectroscopic point of view, inorganic up-conversion materials doped with Ln^{3+} ions are very attractive as they show narrow emission bandwidths and relatively long excited-state lifetimes [8]. Moreover, they exhibit high chemical and optical stability in comparison to phosphors based on organic compounds which tend to undergo photobleaching and photodegradation. Moreover, RE-based inorganic matrices (RE, rare earth, e.g. Y, La, Gd), including fluorides are predominantly low- or non-toxic [9–11] when compared to QDs containing hazardous to health heavy metal ions e.g. Cd^{2+} [12,13]. For this reason, the materials based on RE elements are widely studied.

One of the most frequently studied up-converting dopant system is Yb^{3+}/Er^{3} ion pair, where Yb^{3+} ion acts as a sensitizer excited by infrared radiation, and Er^{3+} ion is an emitter [14]. Generally, there are several mechanisms of up-conversion emission and in this particular case of Yb^{3+}/Er^{3+} ions the mechanism involved is the energy transfer upconversion (ETU)[15]. It is based on absorption of two low energy photons by two neighbouring Yb^{3+} ions, then non-radiative energy transfer from the excited energy level of donors (Yb^{3+} ions) to the excited energy level of the acceptor (Er^{3+} ions) and finally emission of a high energy photon [16,17]. The Er^{3+} ions' emission spectra consist mainly of three bands corresponding to the following transitions $^{2}H_{11/2}\rightarrow{}^{4}I_{15/2}$, $^{4}S_{3/2}\rightarrow{}^{4}I_{15/2}$ (green; λ = 525 nm, λ = 550 nm) and $^{4}F_{9/2}\rightarrow{}^{4}I_{15/2}$ (red; λ = 660 nm) . In the application in fluorescence labelling in biomedicine and the "optical transmission window" of biological tissues, the green emission is not desired but the single-band red emission is of interest [18]. It enables deeper penetration into the tissues and permits avoiding the side effects, reducing the

sensitivity of bioimaging. In order to tune the emission colour and obtain one-band red up-conversion emission, addition of Mn^{2+} ions can be employed. According to literature, the proper amount of Mn^{2+} ions added to the materials doped with Yb^{3+}/Er^{3} ions, can easily tune the emission colour form green to pure red thanks to the efficient energy transfer between Er^{3+} and Mn^{2+} ions [19,20].

This article is focused on investigation of physicochemical properties and cytotoxicity of CaF_2 structures used as a matrix for the trivalent dopant ions. The fluoride-based matrices are very good candidates for Ln^{3+} ions doping thanks to their low phonon energy which enables minimization of the quenching effect of the excited luminescence levels of Ln^{3+}[21]. Moreover, Ln^{3+} ions have ionic radius similar to that of Ca^{2+} ions and can replace them in the structure. Additionally, fluorides can be doped with foreign ions in a wide range of their concentration, without forming impurities phases [22].

The system CaF_2:Yb^{3+}/Er^{3+} was co-doped with Mn^{2+} ions. In order to synthesize a pure and homogenous product a modified-hydrothermal method was used. Then, the structural and tuneable luminescence properties of the product were examined, taking into account the influence of the d-electron ion concentration, infrared excitation type source and laser power. Finally, the cytotoxicity of the CaF_2-doped materials was assessed as nanoparticles may enter surrounding environment and influence living organisms. The effect may depend on, e.g.: dosage, exposure time and size of studied nanoparticles, as well as surface charge, presence of ligand, doping, coating or surface functionalization[10,23,24]. It has been demonstrated that CaF_2 nanoparticles have relatively low effect on mammalian cells in *in vitro* tests, both cancer and normal ones [21,25,26].

Experimental section

Materials

The substances used were: calcium chloride dihydrate, $CaCl_2*2H_2O$ (Sigma Aldrich, ACS reagent≥ 99%), manganese chloride tetrahydrate, $MnCl_2*4H_2O$ (Sigma Aldrich, ACS reagent≥ 98%), sodium citrate tribasic dehydrate, $C_6H_5Na_3O_7*2H_2O$ (Sigma Aldrich, purum p.a. ≥ 99%) , sodium tetrafluoroborate, $NaBF_4$ (Sigma Aldrich, puriss p.a. ≥ 98%), ytterbium oxide Yb_2O_3, erbium oxide Er_2O_3 (99.99% purchased from Stanford Materials, USA), chloric acid HCl (ultra-pure, Avantor S.A., Poland).

Method of synthesis

A series of CaF_2-doped powders was synthesized in hydrothermal conditions in a Berghof DAB-2 reactor. The synthesis was carried out for 6 hours at temperature T= 200 °C. The CaF_2 matrix was doped with 15% Yb^{3+} , 2% Er^{3+} and x% Mn^{2+} ions (x = 0; 1; 5; 10; 20; 30). The desired concentrations of Mn^{2+} were different from those obtained and on the basis of ICP-OES analysis were determined as: x = 0; 0.7; 2.6; 4.7; 6.0; 7.0, respectively.

The synthesis proceeded as follows.

Firstly, the suitable RE oxides were dissolved in ultra-pure chloric acid, then $RECl_3$ synthesized were diluted with distilled water and 0.5 M solutions of $YbCl_3$, $ErCl_3$ were obtained. The solutions were evaporated three times in order to remove the excess of the acid. The 0.5 M solutions of $MnCl_2$, $CaCl_2$ and $NaBF_4$ were also prepared. Four mmols of sodium citrate tribasic dehydrate were dissolved in distilled water and mixed with stoichiometric volume of $CaCl_2$ solution upon stirring (solution A). Next the desired amounts of $RECl_3$ and $MnCl_2$ solutions (solution B) were mixed. Then, solution B was dropwise added to the solution A. Then, to thus prepared mixture, a fluoride source was added (4 mmol), still upon continuous stirring. The prepared mixture had a volume of about 20 ml and was filled with 10 cm^3 distilled water to obtain a series of solutions of the same volume, which ensured the same pressure in each vessel. The pH was not set using

additional reagents, but the procedure applied implied similar pH ~ 6.7 of each sample. The amounts of the reagents used were calculated assuming that the final product molar amount would be 2 mmol. Finally, the obtained transparent solutions were placed in Teflon vessels and put in an autoclave. After synthesis the reactor was left to cool down. The as-obtained products were collected by centrifugation, washed firstly with water then with ethanol three times and dried at 70 °C for 12 h in air. White powders were grounded in a mortar and then analysed.

Methods of cytotoxicity assessments

In vitro assessment of the nanoparticles' cytotoxicity was made. NIH/3T3 (mouse embryonic fibroblast cells) cell line, were cultured in Dulbecco's modified Eagle's medium (DMEM, Lonza), supplemented with 10% foetal bovine serum (Sigma Aldrich), antibiotic and antimycotic solution (Sigma Aldrich). For the cytotoxicity test, 5x104 cells/cm^2 were seeded at 96-well plates and grown for 24 h at 37 °C and 5% CO_2/ 95% air atmosphere. Afterwards, the cells were incubated for 48 h with several different concentrations of the NPs (200, 100, 50 and 10 μg/ml). Phosphate buffered saline (PBS, LabEmpire) supplementation was used as a control.

The influence of the studied NPs on the cells was investigated by determination of cell density (sulforhodamine B assay) and cell condition and morphology . Sulforhodamine B assay (SRB assay) was made according to (Skehan et al., 1990). In order to attach the cells to plastic substratum, cold 50% TCA (trichloroacetic acid, Sigma Aldrich) were gently added to each well. The plates were incubated at 40C for 1 h. Next, the plates were washed five times with distilled water and 0.4% sulforhodamine B (Sigma Aldrich) dissolved in 1% acetic acid (POCh S.A.) was added. The plates were incubated at room temperature for 0.5 h. At the end of the staining period, SRB was removed and the cultures were quickly washed four times with 1% acetic acid, to remove unbound dye. The cell-bound dye was dissolved with 10 mM unbuffered tris base (POCh S.A.). Optical density at 540 nm was measured using multiplate reader (Tecan,

Switzerland). Each experiment was repeated three times and all samples in each experiment were tested in triplets.

Characterization

X-ray diffraction patterns (XRD) were measured with the use of a Bruker AXS D8 Advance diffractometer in Debyee-Scherrer geometry, with Cu $K_{\alpha 1}$ radiation (1.5406 Å) in the 2θ range from 6 to 60°. The XRD diffractograms were analysed with the use of the reference patterns from the Joint Committee on Powder Diffraction Standards (JCPDS) database. An average crystallite sizes were calculated from the Scherrer equation:

High resolution transmission electron microscope (HRTEM) images and energy-dispersive X-ray spectra (EDX) were taken on an FEI Tecnai G2 20 X-TWIN microscope with an accelerating voltage of 200 kV. Scanning electron microscope (SEM) images were recorded at Hitachi S-3400N with EDS detector Thermo Scientific Ultra Dry. In order to prepare TEM samples a few drops of dispersion containing nanoparticles were placed onto carbon grids and then left for drying. The high resolution TEM (HR-TEM) experiments were performed by means of a High Resolution Jeol ARM 200F microscope equipped with Gatan EELS (electron energy loss spectroscopy) spectrometer at 200 kV of accelerating voltage. The quantitative and qualitative composition of the samples prepared was determined and calculated on the basis of measurements by a Varian ICP- OES VISTA-MPX inductively coupled plasma optical emission spectrometer. The specific surface area was determined by the Brunauere Emmette Teller (BET) method with the use of Quantachrome Autosorb iQ. Luminescence excitation, emission spectra and lifetimes were measured at room temperature with the use of a QuantaMaster™ 40 (Photon Technology International) spectrophotometer equipped with an Opolette 355LD UVDM (Opotek Incorporation) tuneable pulsed laser as an excitation source, with repetition rate of 20 Hz, and a Hamamatsu R928 or R5108 photomultipliers (detectors). Also, the solid-state 980 nm

continuous laser (Dragon Lasers) for the up-conversion measurements was used as the excitation source.

Results

Structural analysis

The CaF_2 materials doped with Yb^{3+}, Er^{3+} and additionally Mn^{2+} ions were produced by a facile hydrothermal method. The parameters of the synthesis, mainly pH of the initial mixture (pH~6.7), suitable concentration of sodium citrate preventing premature precipitation, were established to obtain *in situ* desired materials. Further spectroscopic analysis showed that colour tuning did not lead to pure red colour as reported in literature for other fluoride-based materials [20].Therefore, more detailed structural analysis of the compounds obtained was made to find out why. The quantitative composition of the CaF_2-doped materials based on ICP-OES revealed a significant amount of Na^+ ions in the CaF_2 crystal structure, about 16 mol% of Na^+ ions in each sample synthesized. Moreover, the actual amounts of Yb^{3+} ions were different from those expected, and the amounts of Mn^{2+} ions were significantly lower than expected. Table 1 presents the ICP-OES results. It can be noticed that with increasing Mn^{2+} ions concentration, the discrepancy between the expected and measured amounts increases, similarly as described by Li et al. [27]. According to literature, the incorporation of Mn^{2+} ions into the CaF_2 structure is not as efficient as expected and desired [27]. Comparable results have been obtained for other matrices and a number of ideas have been proposed to explain this phenomenon, e.g. low reactivity of the Mn^{2+} precursor [27,28] or predisposition of Mn^{2+} to incorporation into the cubic instead of hexagonal phase in the case of $NaGdF_4$ matrix [27]. The explanation we propose is the difference in solubility in water between MnF_2 (S = 1.06 g/100g of water at T= 20°) and that of less soluble CaF_2, YbF_3 and ErF_3. The equilibrium between the precipitated products and ions

in the medium requires that a proportionally higher amount of the better soluble components (mainly Mn^{2+} ions) remain in solution.

Table 1. Results of the ICP-OES elemental analysis of the CaF_2–doped samples dissolved in diluted HCl solution. Expected concentration of dopant ions was as follows: 18% Yb^{3+}, 2% Er^{3+}, x Mn^{2+} (x = 0, 1, 5, 10, 20, 30).

Actual amounts of ions in CaF_2:Yb^{3+}, Er^{2+}, x Mn^{2+}[mol %]				
Ca^{2+}	Yb^{3+}	Er^{3+}	Mn^{2+}	Na^{+}
68.0	14.9	1.9	0.0	15.3
66.1	14.8	2.0	0.7	16.4
64.5	15.2	2.1	2.6	15.6
61.6	15.6	2.0	4.7	16.1
59.9	16.6	2.3	6.0	15.2
53.7	19.0	2.6	7.0	17.7

In addition, low level of Mn^{2+} ions incorporation into CaF_2 structure (Mn^{2+} ions prefer 6 or 4 coordination number) can be explained by low compatibility of these ions to eight coordinated Ca^{2+} ions, in contrast to Ln^{3+} ions whose most common coordination number is 8 [29]. Furthermore, the substitution of Ca^{2+} ions by Yb^{3+} and Er^{3+} occurs easily because of their similar ionic radii and despite the ion charge imbalance. Furthermore, the charge compensation can explain the presence of Na^{+} in the structure, which play a charge compensator role and can easily replace Ca^{2+} ions of similar ionic radius, which is 1.12 Å and 1.18 Å for Ca^{2+} and Na^{+} , respectively, both in 8-fold coordination, [30,31]. Unexpectedly high concentration of Na^{+} ions

in the samples may be additionally increased as a result of the surface modification of the nanoparticles with trisodium citrate, used as a complexing agent. The coverage of particular nanocrystals and in general sub-microspheres with organic compound was confirmed by the IR spectra presented in Fig. S1 The spectra of the CaF_2–doped samples present absorption bands typical of trisodium citrate and water molecules [25,31–33].

The structure of the CaF_2:15%Yb^{3+}, 2%Er^{3+}, x%Mn^{2+} materials obtained was characterized on the basis of XRD diffractograms (Fig. 1 left). All the samples crystallized in cubic crystal system with space group $Fm\bar{3}m$. Comparison to the reference pattern, JCPDS No. 35-0816, reveals the lack of additional lines, which implies the absence of foreign phases. The crystallinity of the phosphors obtained is high as follows from the intense peaks observed in the XRD patterns. However, a deeper analysis of magnified particular peaks (line 111, as an example, Fig. 1 right) indicates some discrepancy. The XRD lines showed broadening, asymmetry and shift of their maxima towards lower or higher angels, without any regular dependence. These aberrations indicate slight changes in the crystal structure due to doping (Table S1). Firstly, when doping with up to 2.6% of Mn^{2+}, the host lattice parameters have the same values (Fig. 1 right, inset), indicating the lack of noticeable changes in the crystal structure, as expected because Ca^{2+} ions (1.12 Å) are replaced with Mn^{2+} and Yb^{3+} or Er^{3+} ions of smaller ionic radii 0.96 Å, 0.985 Å , 1.004 Å , respectively [30]. When the Mn^{2+} concentration reached 4.7%, the host lattice begun to shrink [34]. The opposite situation was observed when the concentration of the Mn^{2+} ions reached 6.0%, then the calculated lattice parameters indicate the crystal cell expanding probably due to more Mn^{2+} and F^- in the interstitial positions [35].

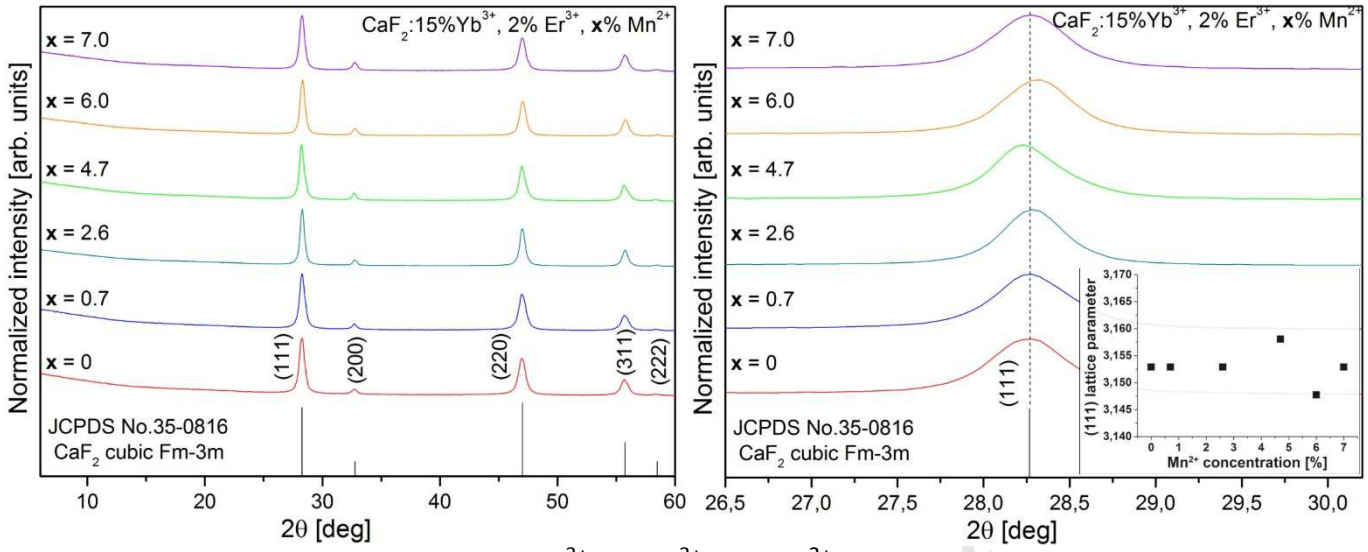

Fig. 1 XRD patterns of the CaF_2:15%Yb^{3+}, 2%Er^{3+}, x%Mn^{2+} (left) and magnification of the reflex (111) (right).

On the basis of the broadened peaks observed on the XRD diffractograms, the average size of the crystallites in the nanometric scale was estimated. Additionally, the result obtained from the calculation with the Scherrer equation partly confirmed this estimation (Table S2.) [36]. Furthermore, SEM images show that the nanocrystallites of CaF_2:15%Yb^{3+}, 2%Er^{3+}, x%Mn^{2+} are the building blocks of the homogenous sub-micrometric spheres (Fig. S2). The 30-50 nm CaF_2-doped nanoflakes formed sub-microspheres with the size changing from 300 to 800 nm, upon increasing Mn^{2+} ions concentration. It is quite a typical behaviour of the CaF_2-based compounds synthesized in hydrothermal conditions in the presence of trisodium citrate (Fig. 2) [11,37,38]. As shown in dark field and TEM images (Fig.2, Fig. S3 (a and b)), increasing content of Mn^{2+} ions and at the same time Yb^{3+} ions, resulted in decreasing average size of the spheres from 760 nm to 250 nm and also in changes in the packing density of nanocrystallites. This relation is probably a result of charge compensation by interstitial F^- ions whose increasing concentration destroys the structure and stability of the crystallites and simultaneously decreases the tendency to aggregation [39]. Moreover, when Mn^{2+} ions concentration increases, the content of Yb^{3+} and

Er^{3+} ions in the structure is rising, so the charge compensation decreases. Then, more F^- anions are induced to compensate the charge and dipoles are formed when the negative charge is on the surface of the crystallites. Therefore, the negative charged crystallites repel each other, and sub-microspheres are not as dense and big as those without Mn^{2+}.

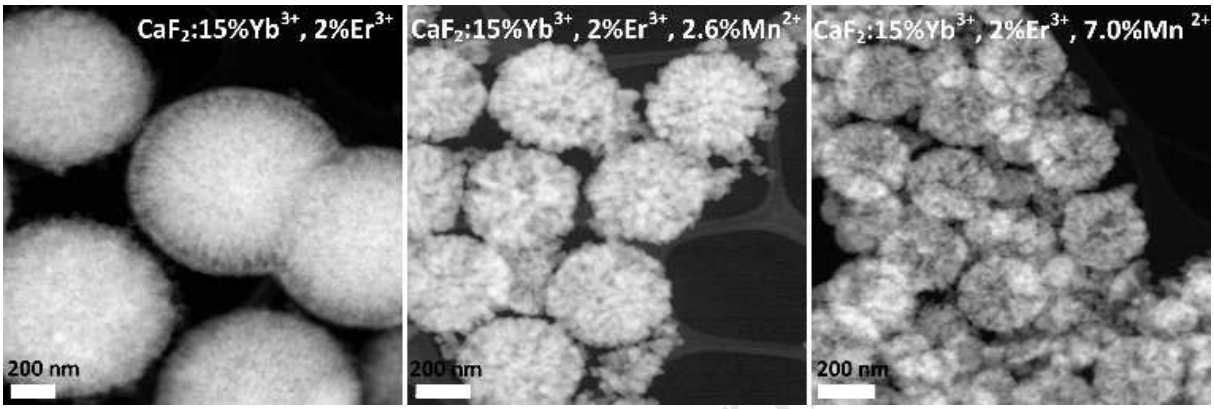

Fig. 2 Dark field images of CaF_2:15%Yb^{3+}, 2%Er^{3+} (a), CaF_2:15%Yb^{3+}, 2%Er^{3+}, 2.6%Mn^{2+} (b) and CaF_2:15%Yb^{3+}, 2%Er^{3+}, 7.0%Mn^{2+} submicrospheres synthesized under hydrothermal conditions in the presence of trisodium citrate.

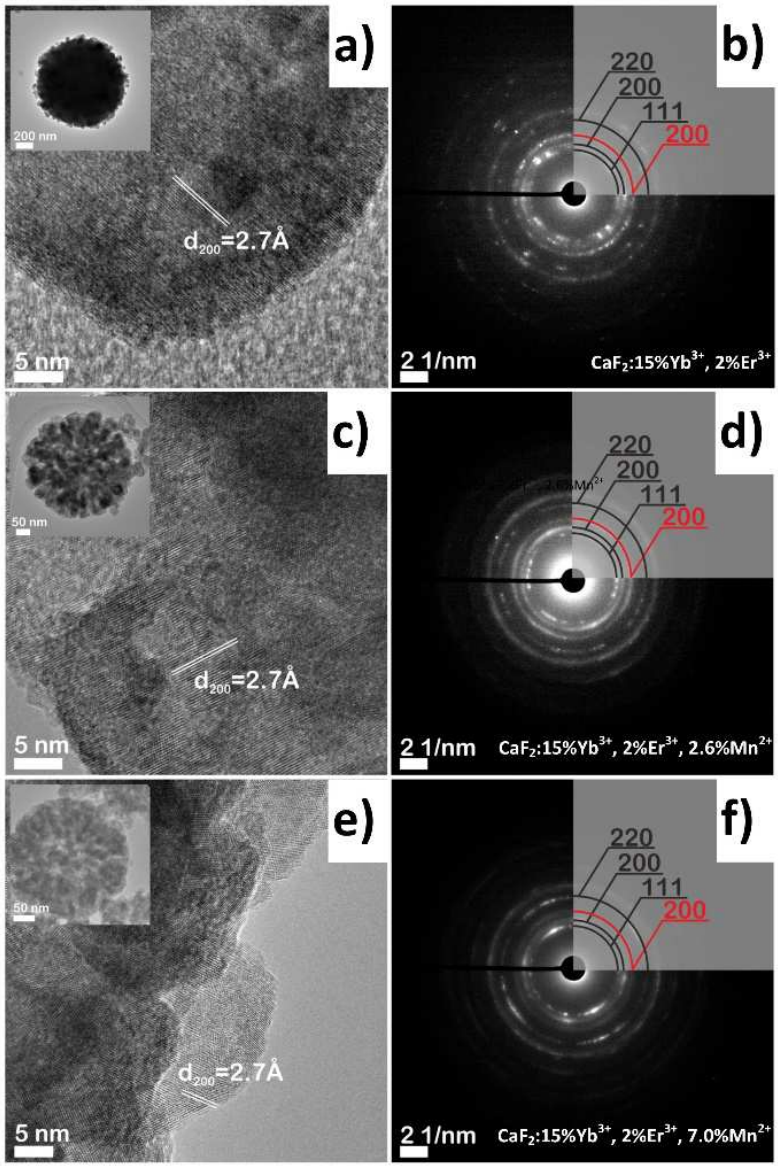

Fig. 3 . HRTEM images (a, c, e) and SAED diffraction patterns (b, d, f) of CaF_2:15%Yb^{3+}, 2%Er^{3+} CaF_2:15%Yb^{3+}, 2%Er^{3+}, 2.6%Mn^{2+} and CaF_2:15%Yb^{3+}, 2%Er^{3+}, 7.0%Mn^{2+}samples, respectively.

The chemical composition of the samples obtained was confirmed by EDX analysis (Fig. S3 (c and d) and the presence of Ca^{2+}, Yb^{3+}, Er^{3+}, Mn^{2+} ions was proved. An additional signal from Na^{+} ions is also noticed, which is consistent with previous information related to the surface modification by sodium citrate and incorporation of these ions into the CaF_2 crystal structures.

In order to analyse the atomic structure of CaF_2:15%Yb^{3+}, 2%Er^{3+}, x%Mn^{2+} samples, the HRTEM and SAED experiments were performed. It was found that the samples obtained were highly crystalline and the lattice planes (200) with characteristic distance of about 2.7Å were identified (Fig. 3 (a, c, e). Nevertheless, individual nanoparticles exhibited polycrystalline morphology particularly in the sample CaF_2:15%Yb^{3+}, 2%Er^{3+}, 7.0%Mn^{2+} (Fig. 3 (e, f)). The remarkable difference in contrast in HRTEM images of studied EELS (Fig. 4 (a-f)) was used to investigate chemical composition of the produced material especially in terms of its elemental homogeneity. On the basis of previous HRTEM observations, the stochastic and non-uniform distribution of elements being the components of the structure was predicted and consequently confirmed by EELS mapping. What is more, the core@shell like structure of nanoparticles was observed i.e. the higher intensity of Ca and O signal coming from the outer part of nanoparticles was evident. It is in accordance with HRTEM and SAED results showing the existence of CaO phase that may be considered as the amorphous outer layer of nanoparticle. The EELS experiments also showed that Mn^{2+} ions are incorporated over the volume of the whole nanoparticle and may accumulate in some areas forming more Mn^{2+} ions doped areas.

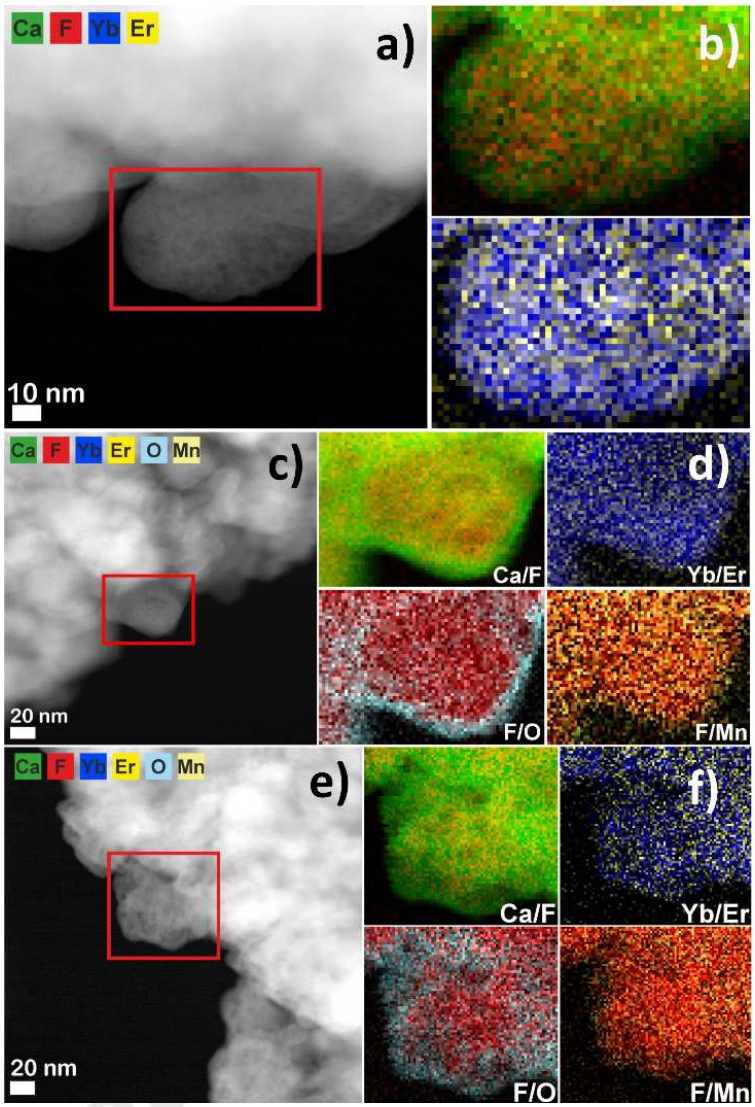

Fig. 4 Dark Field image (a, c, e) and EELS mapping (b, d, f) of CaF_2:15%Yb^{3+}, 2%Er^{3+}(a, b), CaF_2:15%Yb^{3+}, 2%Er^{3+}, 2.6%Mn^{2+} (c, d), CaF_2:15%Yb^{3+}, 2%Er^{3+}, 7.0%Mn^{2+} (e, f) samples.

In order to confirm the presence of particular elements but also to identify the additional impurity CaO phase on the surface, the XPS analysis of the sample CaF_2:15%Yb^{3+}, 2%Er^{3+}, 4.7 %Mn^{2+} was carried out in the range from 200 to 1300 eV (Fig. S4) [40]. The binding energy was

corrected to C1s line of carbon assigned to 284.8 eV. Fig. S4 (a) shows the lines that confirm the presence of all expected elements, including sodium, in accordance with ICP-OES analysis. Figs. S4 (b-f) present high resolution scans of the energy regions specific of each component of CaF_2-doped samples. The calcium high resolution spectrum shows the $Ca2p_{3/2}$ peak, which consists of two components, centred at 350.7 eV and 351.2 eV, assigned to the presence of CaF_2 and CaO, respectively [41](Fig. S4 (b)). Also, a line at 354.7 eV typical of $Ca2p_{1/2}$ is observed. What is more, the peaks related to Ca are significantly shifted in comparison to the CaF_2 reference, probably as a result of Ca-O or Ca-OH bond formation [40]. Fig. S4 (c) shows the deconvoluted F1s line, which exhibits two components. It is explained by different chemical environment of fluorine in the structure [40]. The porosity of the samples prepared was confirmed by the BET analysis of the CaF_2:15%Yb^{3+}, 2%Er^{3+} and CaF_2:15%Yb^{3+}, 2%Er^{3+}, 2.6%Mn^{2+} sub-microspheres, in good agreement with the HR-TEM and SEM images (Fig. S5). The shape of the curves in both cases is characteristic of type IV isotherms with H1 hysteresis loops, which means that the materials have mesoporous structure [11,37,42]. The detailed data related to the BET surface area and total pore volume and diameters are summed up in Table S3.

Luminescence analysis

The spectroscopic properties were characterized on the basis of the excitation spectra, measured by observing the maximum of the red emission band, related to the $^4S_{3/2} \rightarrow {}^4I_{15/2}$ transition, at λ_{obs} = 536 nm (Fig. 5 (a)). The spectra of all prepared samples showed broad and intense excitation bands related to the Stark levels transitions between the $^2F_{7/2}$ and $^2F_{5/2}$ levels of Yb^{3+} ions. High broadening of the $^2F_{7/2} \rightarrow {}^2F_{5/2}$ band corresponds to the nanosize of the building blocks and polycrystalline character of the CaF_2-doped sub-microspheres, as well as high concentration of Yb^{3+} ions which enhances significantly a disorder of environment of the Yb^{3+} ions in the structure [31].

According to literature, Yb^{3+} ions can occupy mainly three sites in the CaF_2 crystal structure: tetragonal C_{4v}, trigonal C_{3v} and cubic O_h [43]. However, these three isolated types of symmetry sites can be clearly spectroscopically detected only at low concentration of trivalent dopant ions (<1mol%), when F^- ions occur in the structure next to nearest neighbour cation in order to compensate the charge imbalance [43–45]. Then, depending on the crystal location of Yb^{3+} ions, the dominance of different bands in the excitation spectra can be observed. However, high concentration of Yb^{3+} in CaF_2-doped samples (<19% of Yb^{3+}) induced the clusters formation. Hence, there is a huge number of structural possibilities, which make it highly difficult to separate them in the spectra, which is additionally emphasized by strong electron–phonon coupling mixing both electronic and vibrionic transitions [43].

For all samples, besides the typical intense band at 976 nm connected with the hexameric clusters RE_6F_{37} of Yb^{3+} ions [46], an additional shoulder at 966 nm is clearly visible which can be assigned to the fact of prevalent occupation of one of the three mentioned above symmetry sites in the clusters. It has been proved that the assignment of particular lines to possible symmetries by classical optical measurements for samples with high concentration of Yb^{3+} ions is ambiguous [45]. Probably, it is assigned to the prevalent occupation of the cubic O_h sites by Yb^{3+} ions [44,45]. For the sample CaF_2 :15% Yb^{3+} , 2% Er^{3+}, 2.6 Mn^{2+} the most prominent excitation line with a maximum at λ = 966 nm was measured, instead of a typical line at 976 nm. This observation can be interpreted as the effect of Na^+ ions which stabilize O_h position of Yb^{3+} ions [31]. According to the ICP-OES results (Table 1) for the sample CaF_2 :15% Yb^{3+} , 2% Er^{3+}, 2.6 Mn^{2+} the contents of Yb^{3+} and Na^+ ions and also Er^{3+} and Mn^{2+} ions are most similar and probably the charge balance of the Yb^{3+} ions is the highest in comparison to the remaining samples, which results in the enhancement of the 966 nm band. Probably, this composition is ideal for stabilization of the O_h site symmetry of Yb^{3+} ions, and enhancement of the 966 nm excitation

band. Generally, the highest intensity of the excitation band was obtained for the sample doped with 2.6% of Mn^{2+} ions.

The emission spectra were measured with the use of two different NIR radiation sources: solid-state continuous laser (λ_{exc} = 980 nm) and pulsed laser (tuneable beam, here λ_{exc} = 980 nm and λ_{exc} = 966 nm were applied) (Fig. 5 (b-d)). The reason for employing different excitation sources was different emission colour observed, depending on the laser type. In both cases, the characteristic emission lines corresponding to the transitions $^2H_{11/2}\rightarrow{}^4I_{15/2}$, $^4S_{3/2}\rightarrow{}^4I_{15/2}$, $^4F_{9/2}\rightarrow{}^4I_{15/2}$ in Er^{3+} ions were observed. Additionally, upon excitation with λ_{exc} = 966 nm a weak band corresponding to the transition $^2H_{9/2}\rightarrow{}^4I_{15/2}$ was noted (Fig. 5 (b)). However, the use of the pulsed laser resulted in green emission with the dominant band at 536 nm, in the whole range of Mn^{2+} ions concentration used (Fig. 5 (c,d)). In this case, tuning of the luminescence colour with increasing concentration of the Mn^{2+} ions was almost unnoticeable. The explanation may be a back energy transfer from red energy level of Er^{3+} to Yb^{3+} or Mn^{2+} ions, which resulted in increased intensity of the green emission of the sample [47]. Otherwise, when the continuous laser was used, changes in the emission colour, from green through orange-red to red were seen with increasing Mn^{2+} ions' concentration [27]. The maximum of the emission was measured at 653 nm in the red region of visible luminescence, and increasing concentration of Mn^{2+} ions caused changes in the I_R/I_G ratio (Fig. 6). Generally, in both cases, upon pulsed and continuous laser excitation, the overall luminescence of the materials synthesized increased with Mn^{2+} ions' concentration increasing up to 2.6%, then decreased with Mn^{2+} ions concentration increasing up to 7.0%. In the entire range of Mn^{2+} ions doping the green band assigned to $^4H_{11/2}\rightarrow{}^4I_{15/2}$ appears. It means that the energy transfer between the $^4T_1$ state of Mn^{2+} ions and the $^4S_{2/3}$ state of Er^{3+} ions is not as efficient as expected, similarly to the phenomenon observed in $NaYbF_4$:Mn^{2+}/Er^{3+} described by Tian et al. [48]. This behaviour may be the effect of the mismatch

of the $^4T_1$ level of Mn^{2+} ions and the excited levels of Er^{3+} ions, as described by Wu et al. for various matrices [49].

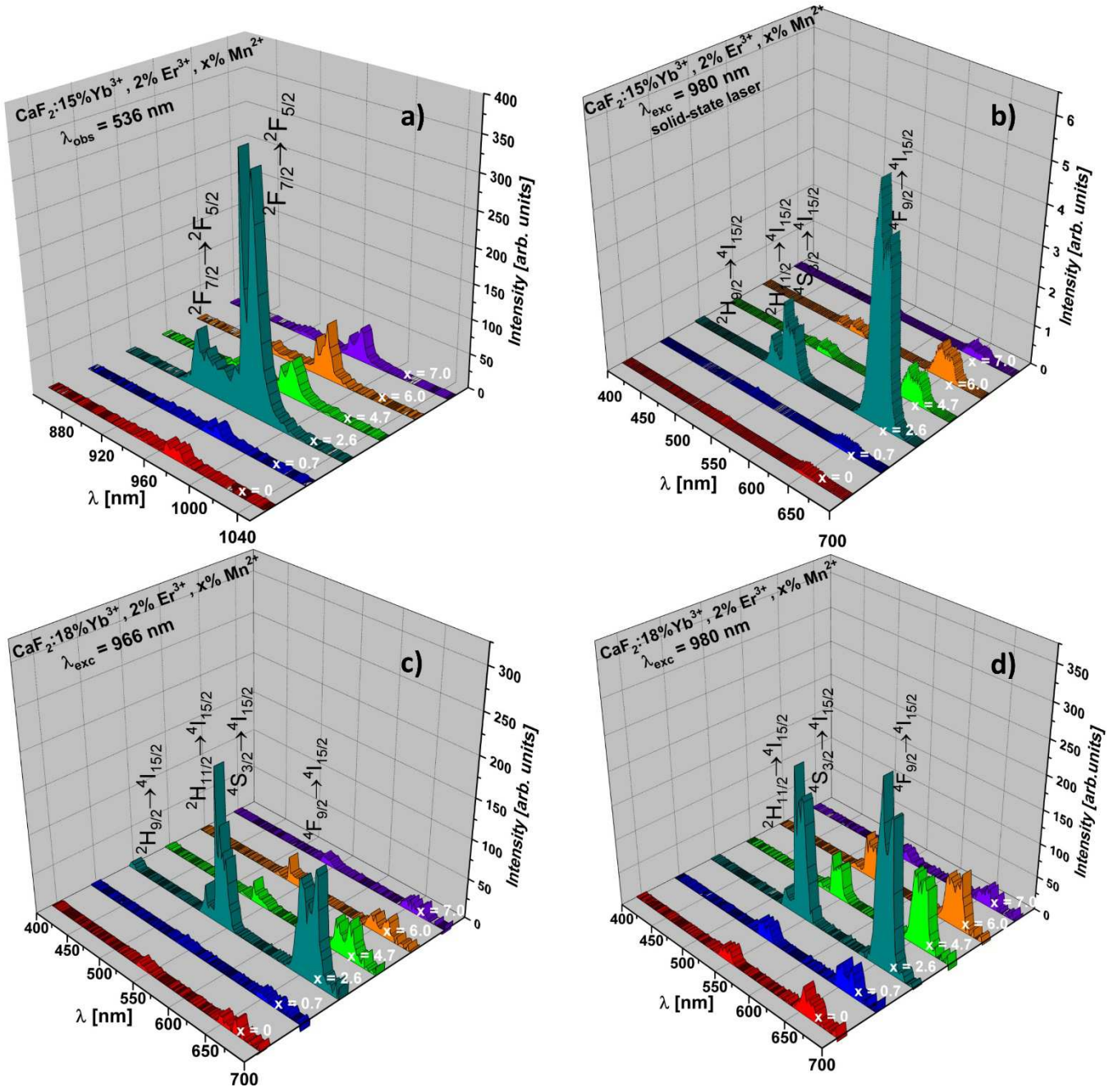

Fig. 5 Excitation spectra (pulsed laser), λ_{obs} = 536 nm (a), emission spectra (solid-state continuous laser), λ_{exc} = 980 nm (b) and emission spectra (pulsed laser), λ_{exc} = 966 nm and λ_{exc} = 980 nm (c,d) of CaF_2- doped samples.

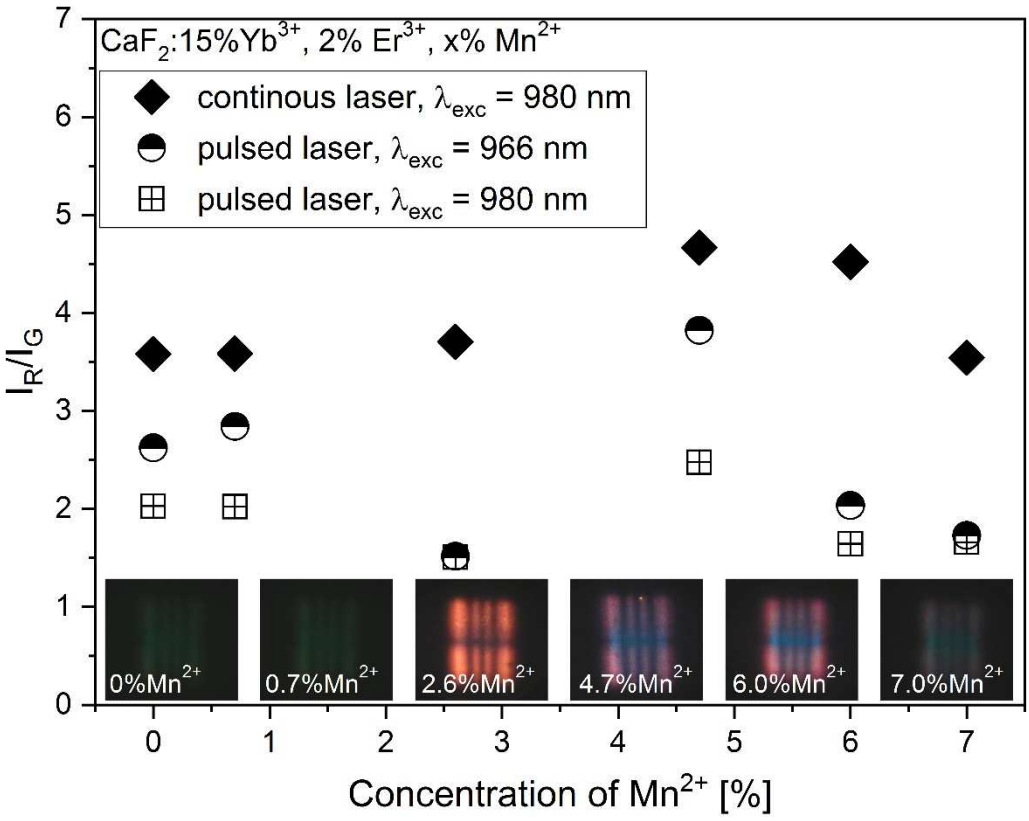

Fig. 6 Dependence of I_R/I_G ratio on Mn^{2+} ions concentration calculated for different excitation sources: solid-state continuous laser and pulsed laser; λ_{exc} = 980 nm.

Spectroscopic characterization was completed by luminescence lifetimes measurements in order to analyse the dependencies on the excitation wavelength and concentration of Mn^{2+}ions. The decay curves shown in Fig. S6 were recorded upon excitation with λ_{exc} = 966 and 980 nm wavelengths. At the same time, the observation wavelengths were chosen to be the most intense emission bands at λ_{obs} =520 nm, 536 nm and 653 nm and, attributed to the transitions $^2H_{11/2}\rightarrow{}^4I_{15/2}$, $^4S_{3/2}\rightarrow{}^4I_{15/2}$ and $^4F_{9/2}\rightarrow{}^4I_{15/2}$, respectively. The decay curve of luminescence lifetimes was exponential in character. For this reason, the effective lifetimes were determined from the following equation :

$$\tau_{eff} = \frac{\int_0^\infty tI(t)dt}{\int_0^\infty I(t)dt} \quad (1)$$

where τ_{eff} is the effective decay time, I(t) is the intensity at time t [50].

Table 2. Calculated effective luminescence lifetimes of the sample CaF_2:15%Yb^{3+}, 2%Er^{3+}, x%Mn^{2+}.

x% Mn^{2+}	**0**	**0.7**	**2.6**	**4.7**	**6.0**	**7.0**
Wavelength	**Lifetime [µs]**					
λ_{exc} = 980 nm λ_{obs} = 520 nm	15.95	16.27	30.61	16.89	16.90	14.57
λ_{exc} = 980 nm λ_{obs} = 536 nm	13.94	12.92	30.48	16.90	16.81	14.41
λ_{exc} = 980 nm λ_{obs} = 653 nm	43.99	47.71	117.61	75.50	54.45	40.26
λ_{exc} = 966 nm λ_{obs} = 520 nm	22.18	17.02	34.16	19.12	19.04	16.24
λ_{exc} = 966 nm λ_{obs} = 536 nm	16.10	16.04	41.08	18.91	19.53	16.02
λ_{exc} = 966 nm λ_{obs} = 653 nm	47.07	51.77	127.93	83.15	64.62	44.55

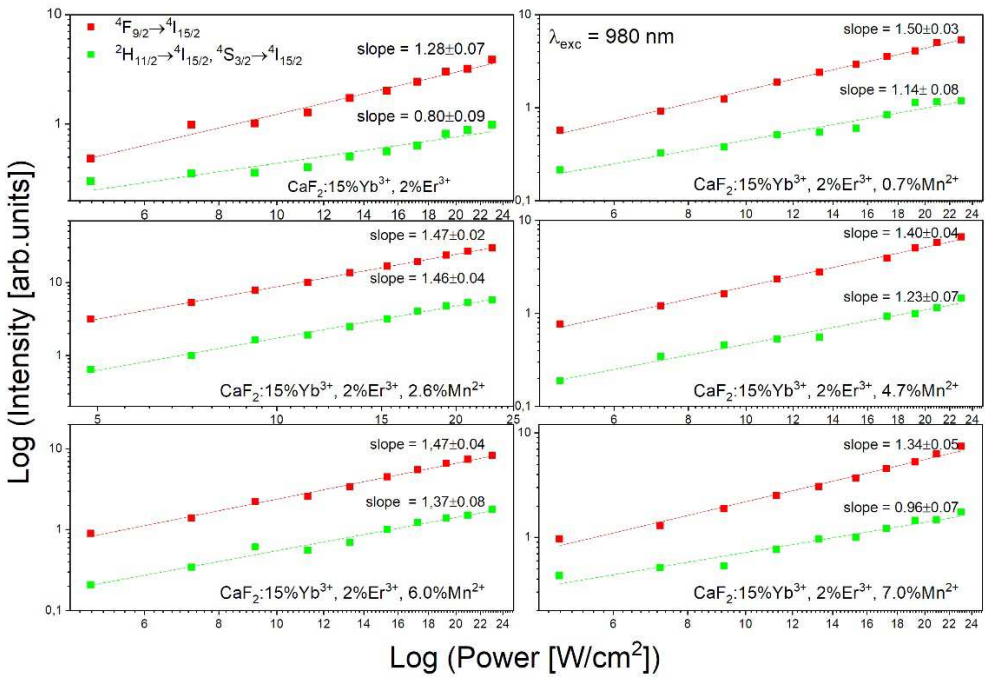

394

395 Fig. 7 Log-log plot of the up-conversion luminescence intensities as a function of the laser power

396 excitation, λ_{exc} = 980 nm.

397

398 The calculated values of the effective luminescence lifetimes are presented in Table 2. The

399 lifetimes measured for the red emission at λ_{obs} = 653 nm observation are much longer when

400 compared to those of the green luminescence at λ_{obs} = 520 nm and λ_{obs} = 536 nm. Generally, for

401 up-converting materials longer lifetime are interpreted as a result of a higher energy transfer

402 rate from other levels to the emission level. The red emission lifetime of Er^{3+} may be a

403 consequence of the energy transfer process from Mn^{2+} to Er^{3+} ions [51]. This phenomenon is

404 associated with the competition between the transition between Mn^{2+} and Er^{3+} ions and

405 radiation emission, which probability increases simultaneously with decreasing local symmetry

406 after addition of Mn^{2+} ions. When the energy transfer between Mn^{2+} and Er^{3+} ions is more

407 competitive, the lifetime of luminescence increases and if the radiation emission is more

408 competitive the luminescence lifetime shortens [52]. The lifetimes upon 966 nm excitation were

409 slightly longer than those measured upon 980 nm excitation. Connecting this result with red

emission lifetime and I_R/I_G ratio, it can be concluded that the excitation with 966 nm promotes red emission and at the same time longer lifetime, and its higher contribution to the whole emission finally gives longer lifetime due to the "forbidden" energy transfer to Yb^{3+} ions at O_h symmetry sites. This symmetry is characterized by highly disordered environment of Ln^{3+} ions, which can probably increase the lifetimes of Er^{3+} emission connected with excitation of Yb^{3+} ions at the sites of this symmetry. Another tendency is that the emission lifetimes increase with the Mn^{2+} concentration increasing up to 2.6% and then rapidly decrease. The longest luminescence lifetimes were calculated for the sample doped with 2.6% Mn^{2+} ions, regardless of the excitation wavelength and emission band observed. This phenomenon can be connected to the fact that for Mn^{2+} ions concentration of 2.6% the ideal system is obtained in which the concentrations of Mn^{2+} and Er^{3+} ions are very similar and competition of energy transfer between their energy level is the highest. Hence, the lifetimes are the longest and the emission is the highest. For analysis of the emission processes, the intensity of luminescence was measured as a function of

the laser power and interpreted assuming the rule $I_{UCL} \propto I_p^n$, where I_{UCL} is the emission intensity and I_p is the pump power. The results were expressed as slopes (Fig. X) of the dependencies of

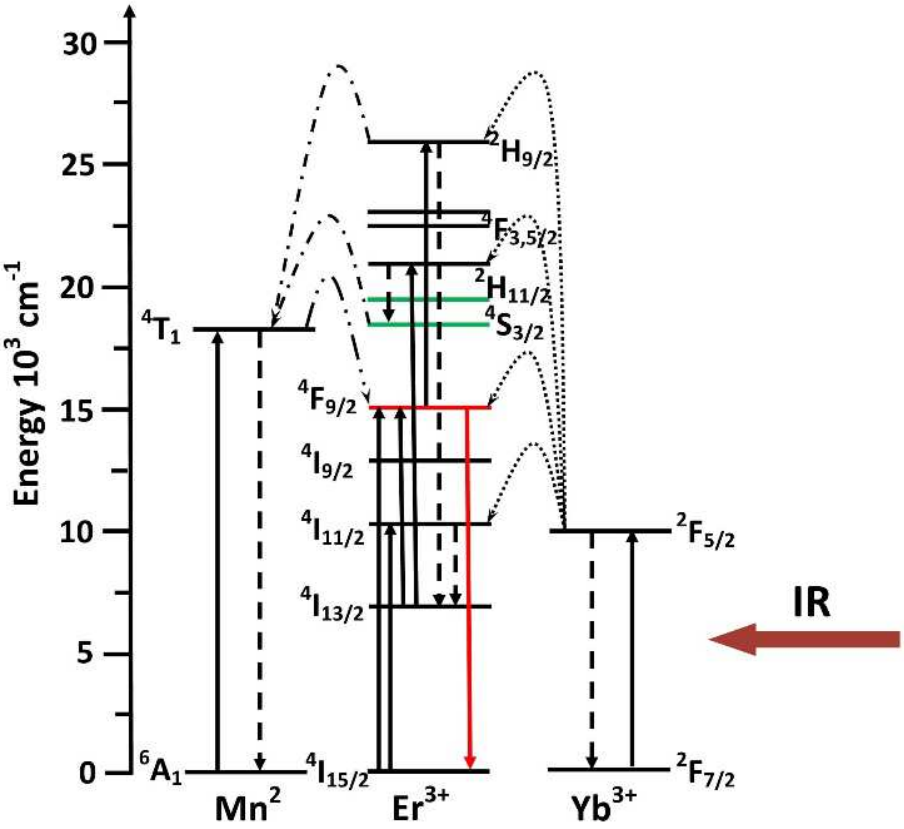

log(laser power per cm2) on log(emission intensity). Generally, Fig. 7 shows curves of the intensity of luminescence at 536 nm ($^2H_{11/2} \rightarrow {}^4I_{15/2}$ transition, green squares) and 653 nm ($^4S_{3/2} \rightarrow {}^4I_{15/2}$, red squares) vs laser power. The slopes of these curves are about 1.5, which indicates two photon process of the weak green and intense red emission of Er^{3+} ions, which is typical of the up-converting materials [53–55]. No particular tendency in changes of in the slope of the above dependencies was observed with increasing Mn^{2+} ions. The obtained slopes, especially for the green emission are obviously smaller than 2, which is probably due to the large depopulation rate of intermediate energy state in the UC process induced by forward and backward energy transfer among Er^{3+}, Yb^{3+} and Mn^{2+} ions [56].

Fig. 8 Scheme of the energy levels and proposed mechanism of energy transfer between Yb^{3+}, Er^{3+} and Mn^{2+} dopant ions in the CaF_2 host matrix.

On the basis of literature reports and detailed luminescence characterization, a mechanism of energy transfer in the tri-doped system with Yb^{3+}, Er^{3+} and Mn^{2+} ions is proposed and schematically presented in Fig. 8. Upon excitation with IR λ_{exc} = 966 or 980 nm wavelengths, Er^{3+} ions are excited through the energy transfer from the $^2F_{5/2}$ excited level of Yb^{3+} ions which as the sensitizers absorb the IR radiation. According to Wu et al., higher energy levels of Mn^{2+} ions promote the green emission and its lower energy levels enhance the red luminescence [49]. For the materials discussed in this article, the increasing content of Mn^{2+} ions resulted in a simultaneous rise of red and green emission band with Mn^{2+} ions concentration increasing up to 2.6% and then decreased up to the Mn^{2+} ions concentration of 7.0%. However, changes in the emission intensity were definitely more significant for the transition $^4F_{9/2}\rightarrow{}^4I_{15/2}$ than for $^2H_{11/2}$, $^4S_{3/2}\rightarrow{}^4I_{15/2}$. It can be concluded that the energy transfer (ET) between Mn^{2+} and Er^{3+} ions is clearly visible and at the same time, the most efficient transfer takes place between the $^4T_1$ excited level to $^4F_{9/2}$ level than to $^2H_{11/2}$ and $^4S_{3/2}$ levels, especially for the sample CaF_2:15%Yb^{3+}, 2%Er^{3+},2.6 %Mn^{2+}. Hence, it can be established that $^4T_1$ excited level of Mn^{2+} ions is located between the excited levels $^4F_{9/2}$ and $^2H_{11/2}$, $^4S_{3/2}$ of Er^{3+} ions, but closer to the red one. This is the reason for more efficient energy transfer to the level $^4F_{9/2}$ and relaxation to the ground state $^4I_{15/2}$ of Er^{3+} ions and for observation of intense red emission. Next, electrons can be excited to the levels $^4F_{9/2}$ and $^2H_{11/2}$, $^4S_{3/2}$ by the excited state absorption (ESA) and simultaneously by ET from $^4I_{11/2,}$, followed by relaxation to $^4I_{15/2}$ and give red and green emission, respectively. Back transfer is also possible, from green excited energy level of Er^{3+} to the excited level $^4T_1$ of Mn^{2+} ions, which resulted in quenching of green emission.

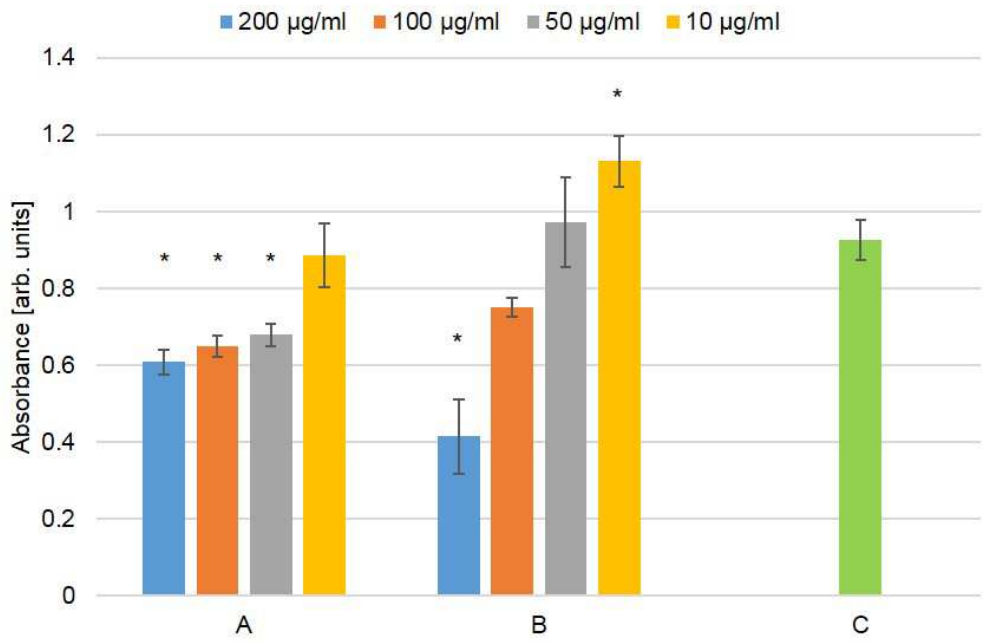

458 Fig. 9. Viability of NIH/3T3 cells, evaluated by SRB assay, treated with the following
459 nanoparticles: A. CaF_2:15%Yb^{3+}, 2%Er^{3+}, 2.6%Mn^{2+}, B. CaF_2:15%Yb^{3+}, 2%Er^{3+}, C. control. Each of
460 the samples is presented with the subsequent concentrations: 200 µg/ml, 100 µg/ml, 50 µg/ml
461 and 10 µg/ml. Control cell cultures were supplemented with adequate volume of PBS. Asterisks
462 indicate the results significantly different from those obtained for the control (ANOVA).

463 **Cytotoxicity**

464 In order to estimate of the nanocrystals' cytotoxicity, cell proliferation studies in *in vitro* cultures
465 of the fibroblast were examined (Fig. 9). The results suggested that CaF_2:15%Yb^{3+}, 2%Er^{3+},
466 2.6%Mn^{2+} reduces cell viability at a lower concentration than CaF_2:15%Yb^{3+}, 2%Er^{3+}. Namely, the
467 proliferation rate of the cells incubated with the calcium fluoride doped with manganese at
468 concentrations: 200, 100 and 50 µg/ml were statistically lower than in the control cells.
469 Whereas, calcium fluoride without manganese decrease the cell viability only at the
470 concentration 200 µg/ml. It confirms the previous observations that Mn^{2+} ions may increase cell
471 mortality [57]. Calcium fluoride without manganese was not toxic up to 100 µg/ml. What is

interesting, the cells incubated with CaF_2:15%Yb^{3+}, 2%Er^{3+} nanoparticles at 10 µg/ml showed a higher proliferation rate than in the control.

Conclusions

Applying the hydrothermal conditions and sodium citrate as a surfactant, a series of CaF_2 samples doped with Yb^{3+}, Er^{3+} and Mn^{2+} ions was synthesized. The morphology of the materials prepared was defined as sub-microspheres composed of nanocrystallites whose average size was decreasing with the concentration of Mn^{2+} ions increasing , from 300 to 800 nm. On the basis of the XRD results the structures of the obtained samples was determined as pure, without any impurities. However, detailed structural analysis based on HR-TEM images and SAED diffraction supported by EELS mapping permitted identification of a foreign phase in the form of CaO. Moreover, ICP-OES studies showed that Mn^{2+} ions can be not as efficiently as expected introduced into the structure of the host matrix. The analysis of spectroscopic behaviour is complicated due to the presence of a foreign phase and a discrepancy between the expected and desired contents of particular elements.

The use of two different types of excitation source permitted achieving different effects of colour tuning. In fact, noticeable changes in the emission colour were observed for the solid-state continues laser as a excitation source, the colour could be changed from green to orange-red. The most effective composition of the dopant ions concentration, determined on the basis of ICP-OES analysis and luminescence characterization, was that of the ratio of Mn^{2+} to Er^{3+} ions was 1:1, which resulted in long luminescence lifetime and the brightest emission of the highest intensity.

The cytotoxicity of the materials obtained indicated that CaF_2 – doped samples are not toxic for human living cells.

Acknowledgments

The presented results were financially supported by Ministry of Science and Higher Education, Iuventus Plus, 0145/IP2/2015/73.

References:

[1] Y. Zhou, B. Ling, H. Chen, L. Wang, Talanta 180 (2018) 120–126.

[2] X. Liu, Y. Wang, X. Li, Z. Yi, R. Deng, L. Liang, X. Xie, D.T.B. Loong, S. Song, Di. Fan, A.H. All, H. Zhang, L. Huang, X. Liu, Nat. Commun. 8 (2017) 1–7.

[3] Q. Qiang, Y. Wang, New J. Chem. (2018).

[4] N. Wang, Z. Fu, Y. Wei, T. Sheng, J. Alloys Compd. 772 (2019) 371–380.

[5] H. Lu, H. Hao, H. Zhu, G. Shi, Q. Fan, Y. Song, Y. Wang, X. Zhang, J. Alloy. Comp. 728 (2017) 971–975.

[6] H. Huang, J.F. Lovell, Adv. Funct. Mater. 27 (2017) 1603524.

[7] Y. Liu, X. Meng, W. Bu, Coord. Chem. Rev. 379 (2019) 82–98.

[8] M. Ding, M. Xu, C. Lu, J. Xi, Z. Ji, D. Chen, J. Alloy. Comp. 721 (2017) 531–537.

[9] T. Grzyb, L. Mrówczyńska, A. Szczeszak, Z. Śniadecki, M. Runowski, B. Idzikowski, S. Lis, J. Nanopart. Res. 17 (2015) 399.

[10] A. Szczeszak, A. Ekner-Grzyb, M. Runowski, K. Szutkowski, L. Mrówczyńska, Z. Kaźmierczak, T. Grzyb, K. Dąbrowska, M. Giersig, S. Lis, J. Colloid Interface Sci. 481 (2016) 245–255.

[11] X. Deng, Y. Dai, J. Liu, Y. Zhou, P. Ma, Z. Cheng, Y. Chen, K. Deng, X. Li, Z. Hou, C. Li, J. Lin, Biomaterials 50 (2015) 154–63.

[12] A.M. Derfus, W.C.W. Chan, S.N. Bhatia, Nano Lett. 4 (2004) 11–18.

[13] N. Chen, Y. He, Y. Su, X. Li, Q. Huang, H. Wang, X. Zhang, R. Tai, C. Fan, Biomaterials 33 (2012) 1238–1244.

[14] T. Grzyb, S. Balabhadra, D. Przybylska, M. Węcławiak, J. Alloys Compd. 649 (2015) 606–616.

[15] F. Auzel, Chem. Rev. 104 (2004) 139–73.

[16] M. Lin, Y. Zhao, S. Wang, M. Liu, Z. Duan, Y. Chen, F. Li, F. Xu, T. Lu, Biotechnol. Adv. 30 (2012) 1551–61.

[17] D.C. Rodriguez Burbano, R. Naccache, J.A. Capobianco, Near-IR Triggered Photon Upconversion, 1st ed., Elsevier B.V., 2015.

[18] Z. Bai, H. Lin, K. Imakita, R. Montazami, M. Fujii, N. Hashemi, RSC Adv. 4 (2014) 61891–61897.

[19] J. Wang, F. Wang, C. Wang, Z. Liu, X. Liu, Angew. Chem. Int. Ed. 50 (2011) 10369–72.

[20] G. Tian, Z. Gu, L. Zhou, W. Yin, X. Liu, L. Yan, S. Jin, W. Ren, G. Xing, S. Li, Y. Zhao, Adv. Mater. 24 (2012) 1226–31.

[21] J. Zhao, Y.J. Zhu, J. Wu, F. Chen, J. Colloid Interf. Sci. 440 (2015) 39–45.

[22] T. Grzyb, M. Runowski, A. Szczeszak, S. Lis, J. Phys. Chem. C 116 (2012) 17188–17196.

[23] E. Wysokińska, J. Cichos, E. Zioło, A. Bednarkiewicz, L. Strzadała, M. Karbowiak, D. Hreniak, W. Kałas, Toxicol. Vitr. 32 (2016) 16–25.

[24] A. Elsaesser, C.V. Howard, Adv. Drug Deliv. Rev. 64 (2012) 129–37.

[25] S. Sasidharan, A. Jayasree, S. Fazal, M. Koyakutty, S. V. Nair, D. Menon, Biomater. Sci. 1 (2013) 294–305.

[26] W.A. Bala, V.S. Benitha, K. Jeyasubramanian, G.S. Hikku, P. Sankar, S.V. Kumar, J. Fluor. Chem. 193 (2017) 38–44.

[27] X. Li, X. Liu, D.M. Chevrier, X. Qin, X. Xie, S. Song, H. Zhang, P. Zhang, X. Liu, Angew. Chem. Int. Ed. 54 (2015) 13312–13317.

[28] A. Nag, S. Sapra, C. Nagamani, A. Sharma, N. Pradhan, S. V. Bhat, D.D. Sarma, Chem. Mater. 19 (2007) 3252–3259.

[29] G. Malandrino, I.L. Fragalà, Coord. Chem. Rev. 250 (2006) 1605–1620.

[30] R.D. Shannon, Acta Cryst. A 32 (1976) 751–767.

[31] M. Pedroni, F. Piccinelli, T. Passuello, S. Polizzi, J. Ueda, P. Haro-González, L. Martinez Maestro, D. Jaque, J. García-Solé, M. Bettinelli, A. Speghini, Cryst. Growth Des. 13 (2013) 4906–4913.

[32] B. Lakshmanan, J. Indian Inst. Sci. 39 (1968) Suppl:108-120.

[33] C. Pandurangappa, B.N. Lakshminarasappa, B.M. Nagabhushana, J. Alloy. Comp. 489 (2010) 592–595.

[34] T. Fan, J. Lü, G. Li, Y. Huang, Opt. Eng. 56 (2017) 017104.

[35] C. Zhao, X. Kong, X. Liu, L. Tu, F. Wu, Y. Zhang, K. Liu, Q. Zeng, H. Zhang, Nanoscale 5 (2013) 8084–8089.

[36] A. Patterson, Phys. Rev. 56 (1939) 972–977.

[37] C. Zhang, C. Li, C. Peng, R. Chai, S. Huang, D. Yang, Z. Cheng, J. Lin, Chem. Eur. J. 16 (2010) 5672–5680.

[38] Z. Xia, Y. Fu, T. Gu, Y. Li, H. Liu, Z. Ren, X. Li, G. Han, Mater. Des. 119 (2017) 85–92.

[39] A. Bensalah, M. Mortier, G. Patriarche, P. Gredin, D. Vivien, J. Solid State Chem. 179 (2006) 2636–2644.

[40] C. dos S. Bezerra, M.E.G. Valerio, Phys. B Condens. Matter 501 (2016) 106–112.

[41] P. Dolcet, A. Mambrini, M. Pedroni, A. Speghini, S. Gialanella, M. Casarin, S. Gross, RSC Adv. 5 (2015) 16302–16310.

[42] K.S.W. Sing, D.H. Everett, R. a. W. Haul, L. Moscou, R. a. Pierotti, J. Rouquérol, T. Siemieniewska, Pure Appl. Chem. 54 (1982) 2201–2218.

[43] M. Ito, C. Goutaudier, Y. Guyot, K. Lebbou, T. Fukuda, G. Boulon, J. Phys. Condens. Matter 16 (2004) 1501–1521.

[44] V. Petit, P. Camy, J.L. Doualan, R. Moncorgè, J. Lumin. 122–123 (2007) 5–7.

[45] V. Petit, P. Camy, J.L. Doualan, X. Portier, R. Moncorgé, Phys. Rev. B 78 (2008) 1–12.

[46] A.E. Nikiforov, Phys. Solid State 47 (2005) 1431.

[47] M. Kaiser, C. Würth, M. Kraft, I. Hyppänen, T. Soukka, U. Resch-Genger, Nanoscale 9 (2017) 10051–10058.

[48] D. Tian, D. Gao, B. Chong, X. Liu, Dalt. Trans. (2015) 4133–4140.

[49] M. Wu, X.F. Jiang, E.H. Song, J. Su, Z.T. Chen, W.B. Dai, S. Ye, Q.Y. Zhang, J. Mater. Chem. C 4 (2016) 9598–9607.

[50] J.R. Lakowicz, Principles of Fluorescence Spectroscopy, third, Springer, Baltimore, 2006.

[51] Z. Huang, H. Gao, Y. Mao, RSC Adv. 6 (2016) 83321–83327.

[52] E.J. He, H.R. Zheng, W. Gao, Y.X. Tu, Y. Lu, H.N. Tian, G.A. Li, J. Nanosci. Nanotechnol. 14 (2014) 4139–4146.

[53] S. Zeng, Z. Yi, W. Lu, C. Qian, H. Wang, L. Rao, T. Zeng, H. Liu, H. Liu, B. Fei, J. Hao, Adv. Funct. Mater. 24 (2014) 4051–4059.

[54] S. Ye, Y. Li, D. Yu, G. Dong, Q.-Y. Zhang, J. Mater. Chem. 21 (2011) 3735.

[55] X. Xu, Z. Wang, P. Lei, X. Liu, Y. Su, L. Dong, S. Yao, L. Zhou, S. Song, J. Feng, H. Zhang, Dalt. Trans. 44 (2015) 17286–17292.

[56] J.L. Wang, E.H. Song, M. Wu, W.B. Dai, S. Ye, Q.Y. Zhang, Mater. Res. Bull. 74 (2016) 340–345.

[57] F. Mohammad, H.A. Al-Lohedan, J. Mater. Sci. 51 (2016) 9207–9216.

Emission colour changes in the CaF_2 sub-microspheres doped with Yb^{3+}, Er^{3+} and Mn^{2+} ions

Highlights

1) Structural analysis of CaF_2-doped phosphors showed the core@shell like structure
2) The Mn^{2+} ions' quantity in the CaF_2 matrix definitely differs from the expected
3) The emission colour of CaF_2-doped materials was tuned from green to orange – red
4) Two various type of excitation source resulted in different effect of colour tuning

Declaration of interests

☒ The authors declare that they have no known competing financial interests or personal relationships that could have appeared to influence the work reported in this paper.

☐The authors declare the following financial interests/personal relationships which may be considered as potential competing interests: